

A Radiometric Noise Model for Estimating Geometrical Parameters of 3-D Bodies From Multispectral Images

J.C. Glas & F. van der Heijden

University of Twente*, The Netherlands

Abstract

Camera images can be used to measure the geometry of man-made objects. An iterative weighted least-squares estimator with knowledge of imaging and reflection models retrieves the geometrical parameters of objects in a 3-D scene from 2-D image projections. We investigate the use of multispectral imagery which allows us to separate diffuse and specular reflection before estimating geometry. We built a multispectral camera measurement system that has been used to capture real images of a cylindrical body. These have been processed to analyse the propagation of radiometric noise from reflection via imaging into reflection component separation. The purpose of this research is the development of a radiometric noise model for use in our geometry estimator.

1 Introduction

The reflection of light on a surface is based on two major physical phenomena. Diffuse (body) reflection originates from emission of light that has not been absorbed after penetrating the material. Specular (interface) reflection mirrors incident light in opposite direction with a scatter that dilates with surface roughness. The latter component accounts for the occurrence of shiny spots upon curved surfaces. We consider these so called highlights to be useful clues for shape from shading rather than inconvenient image disturbances.

Under the assumption that both reflection components can be separated before estimating geometry, we have shown both analytically [2] and by simulation [1] that the *smooth* profile of the diffuse component provides the estimator with good convergence properties, while the *sharp* profile of the specular component can be utilized to reduce the noise sensitivity of some of the geometrical parameters to be estimated. The noise model applied in these experiments consisted of additive noise on both reflection components with no correlation in between. However, a refinement of this simplistic model is required to provide accurate estimates of geometrical parameters from real images.

A multispectral camera measurement system has been built to capture real images of a cylindrical

body. Its curved surface ascertains the occurrence of a highlight beside a diffuse component that will smoothly vary along the curve. Positioning the light source and camera at a large distance provides a (near)-constant reflection geometry in the direction along the axis of the cylinder. Sampling the multispectral image or its separated reflection components in the direction of the axis enables the estimation of statistical parameters as a function of the varying reflection geometry in the perpendicular direction. Analysis of these statistics must lead to a radiometric noise model for the reflection components of the separated image. For this purpose, we first need to perform the reflection component separation utilizing the multispectrality of our images.

2 Reflection component separation

The reflection from the surface of an object can be considered as a linear combination of diffuse and specular reflection. Inherent differences in the spectral density of these reflection components offer possibilities to separate them in a multispectral image without knowledge of the geometry of the scene. Adopting the *dichromatic reflection model* [3] for inhomogeneous dielectrics (e.g. plastics and paint), the spectral density $F(\mathcal{G}, \lambda)$ of light reflected from a surface can be formulated as

$$F(\mathcal{G}, \lambda) = \alpha_d(\mathcal{G})L(\lambda)R(\lambda) + \alpha_s(\mathcal{G})L(\lambda) \quad (1)$$

where $\alpha_d(\mathcal{G})$ and $\alpha_s(\mathcal{G})$ are the (d)iffuse and (s)pecular weights depending on geometry \mathcal{G} of the scene. Interaction between light and matter makes the spectral density of the diffuse component a product of the spectral density $L(\lambda)$ of the light source and the spectral reflectance $R(\lambda)$ of the surface material. The interface reflection makes the spectral density of the specular component equal the spectral density $L(\lambda)$ of the light source assuming wavelength independence of the Fresnel reflection coefficient.

When the light reflected from a surface falls through a colour filter with spectral transmittance $T_i(\lambda)$ onto a CCD-element of a camera with spectral sensitivity $S(\lambda)$, the spectral irradiance is integrated into a measurable voltage $\theta_i(\mathcal{G})$ proportional to

$$\begin{aligned} \theta_i(\mathcal{G}) &\propto \int_{\lambda} F(\mathcal{G}, \lambda)T_i(\lambda)S(\lambda)d\lambda = \\ \alpha_d(\mathcal{G}) \int_{\lambda} L(\lambda)R(\lambda)T_i(\lambda)S(\lambda)d\lambda &+ \alpha_s(\mathcal{G}) \int_{\lambda} L(\lambda)T_i(\lambda)S(\lambda)d\lambda \\ &= \alpha_d(\mathcal{G})d_i + \alpha_s(\mathcal{G})s_i \end{aligned} \quad (2)$$

The difference in the sensitivity of the sensor for diffuse and specular reflection is tied up in the ratio of

* Department of Electrical Engineering, Control, Systems and Computer Engineering Group, Laboratory for Measurement Science and Instrumentation, P.O. Box 217, 7500 AE Enschede, The Netherlands, Phone: +31 53 489 2785, Fax: +31 53 489 1067, E-mail: jaap@mi.el.utwente.nl

the constants d_i and s_i , so that the precise knowledge of all spectral densities is not required.

Viewing the same geometry \mathcal{G} with filters of different spectral transmittance $T_i(\lambda)$ gives us a measurement vector $\vec{\theta}(\mathcal{G})$ in a multi-dimensional feature space. Vectorization of the corresponding constants d_i and s_i from Eq. (2) provides the diffuse and specular direction vectors \vec{d} and \vec{s} which span a 2-D subspace. The projection of the (noisy) measurement vectors onto this *plane* will determine the separation in reflection components. Vectorization of the diffuse and specular weights $\alpha_d(\mathcal{G})$ and $\alpha_s(\mathcal{G})$ into parameter vector $\vec{\alpha}(\mathcal{G})$ arises the following (over)determined linear inverse problem in matrix-vector form:

$$\begin{aligned} \vec{\theta}(\mathcal{G}) &\propto \alpha_d(\mathcal{G})\vec{d} + \alpha_s(\mathcal{G})\vec{s} = \begin{pmatrix} \vec{d} & \vec{s} \end{pmatrix} \vec{\alpha}(\mathcal{G}) = A\vec{\alpha}(\mathcal{G}) \\ &\Rightarrow \hat{\vec{\alpha}}(\mathcal{G}) \propto (A^T A)^{-1} A^T \vec{\theta}(\mathcal{G}) \end{aligned} \quad (3)$$

A straightforward least-squares estimation [5] provides the estimated weights $\hat{\vec{\alpha}}(\mathcal{G})$ to separate each multispectral measurement $\vec{\theta}(\mathcal{G})$ into reflection components.

2.1 Estimation of diffuse and specular direction

Accurate estimation of the diffuse and specular direction vectors \vec{d} and \vec{s} is essential for a successful reflection component separation. The set of measurement vectors from a surface of uniform reflectance that is partially covered by highlight(s) forms a 2-D subspace in feature space, if the dichromatic reflection model applies. This plane can be estimated by principal component analysis of the covariance matrix of the set of (noisy) measurement vectors. The plane is spanned by the eigenvectors that correspond to the biggest pair of eigenvalues. Planes originating from surfaces of different spectral reflectance but radiated by the same light source must share a 1-D subspace that is spanned by the specular direction vector \vec{s} . An estimate of \vec{s} is obtained by intersecting two of those planes.

If the spectral reflectance of a surface is not white, one can distinguish two joining clusters of measurement vectors in feature space [4] (see examples in Figures 3 and 4). The first cluster points from the origin and contains vectors with negligible specular reflection. The second cluster makes an angle towards the specular direction vector and contains vectors with both a diffuse and a specular reflection component. Principal component analysis can be applied to the covariance matrix of a set of (noisy) measurement vectors that definitely belong to the first cluster. Selection of this subset has been performed manually so far. The estimate of the diffuse direction vector \vec{d} is given by the eigenvector that corresponds to the biggest eigenvalue.

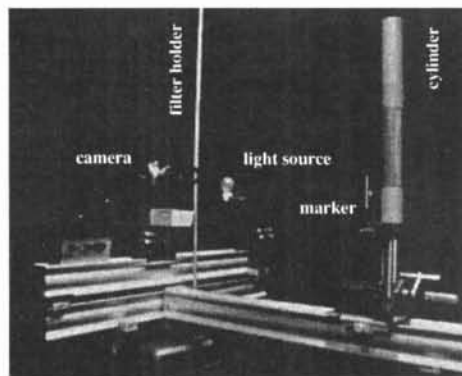


Figure 1: Our multispectral camera measurement system.

3 A multispectral camera measurement system

Figure 1 shows our multispectral camera measurement system. It has been founded on a T-shaped horizontal beam construction. Camera and light source are mounted on and moveable along the shorter beam. An upright standing cylinder with a rotateable and interchangeable jacket surface can be moved along the longer beam. An ordinary 100W incandescent light bulb serves as a distant isotropic point light source. Our camera is a Teli CS8310C monochrome CCD-camera with an Olympus lens of 50mm focal distance. Its images are digitized by a Datacell S2200 framegrabber card plugged into a Sun Sparc-station.

The spectral sensitivity of the camera can be varied by shifting stacks of Schott colour glass filters [6] in front of the lens of the camera. The three stacks used for our measurements respectively contained a 3mm RG665 filter (Red), a 1mm BG7 filter (Blue) and a combined 1mm BG7 on 3mm GG495 filter (Green). Inserting a 3mm KG3 infrared blocking filter in each stack is necessary to have the response of the camera dominated by the visible spectrum in which diffuse and specular reflection differ most.

The post-processing starts with aligning the multispectral bands of the image to correct translations introduced by the different filter stacks. A marker has been added to the scene for this purpose. Next the multispectral image is rotated to align the cylinder axis precisely with the vertical axis of the image. The rotation angle is derived from the prevailing gradient of the image.

4 Experimental results

Multispectral images were captured from the surface of the cylinder that was respectively covered with blue and red plastic sheet of a leather-look roughness. Figure 2 shows the image of the red cylinder taken with the Red filter stack in charge. Figures 3 and 4 show elevation plots of the 2-D histograms of the Red-Blue images of both cylinders.

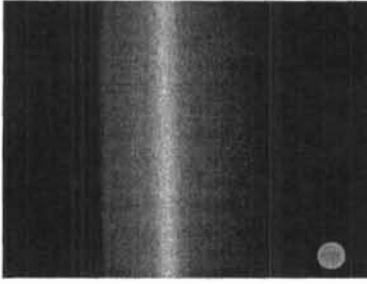


Figure 2: Image of red plastic cylinder (and marker) captured with the Red filter.

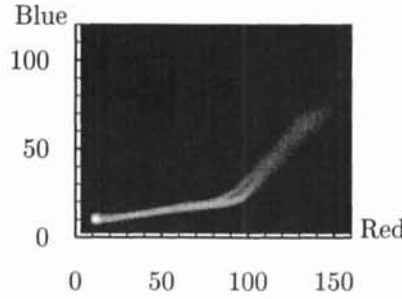


Figure 3: Elevation plot (log) of 2-D histogram of Red-Blue image of red cylinder.

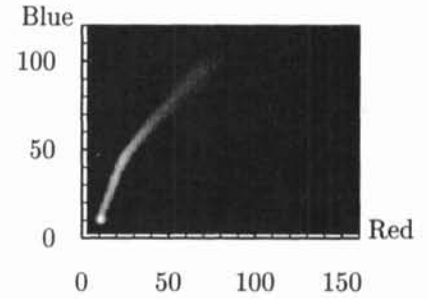


Figure 4: Elevation plot (log) of 2-D histogram of Red-Blue image of blue cylinder.

The bright spots bottom left originate from background pixels. Those histograms have been used for the proper selection of the subsets of 3-D measurement vectors from which the diffuse direction vector \vec{d} of both cylinders and the joint specular direction vector \vec{s} were derived (see § 2.1).

The reflection component separation has been performed on the multispectral images of both cylinders, but we will present the results of the red cylinder only. Figures 5 to 10 show the plots for three statistical parameters: mean, standard deviation and correlation coefficient in vertical direction for all bands of the multispectral image and for the two separated reflection components¹. The successful separation into reflection components appears from the smooth profiles of their mean values in Figure 8. A systematic separation error would appear as a lump or dent in the diffuse profile at the position of the highlight. The absence of such an error is highly dependent on the accurate estimation of \vec{d} and \vec{s} . According as the angle between these vectors is smaller, their estimation will be more difficult in itself and an error will propagate stronger into the separated reflection components. This makes the multispectral separation method less suitable for surfaces with a near-white reflectance.

4.1 Radiometric noise analysis

The influence of the various radiometric noise sources on the multispectral camera measurements appears from the standard deviation in Figure 6. The signal-independent part originates from camera-related sources like dark current noise, amplifier noise and quantization errors [7]. The narrow peak at the left is an artifact caused by the abrupt change from background to object.

The signal-dependent part includes spatial variation in sensitivity of the camera (fixed pattern noise), intensity of the light source, transmittance of the colour filters and spectral reflectance of the surface, which all impose a linear relationship between

¹The magnitude of the mean and standard deviation of the separated reflection components is expressed in terms of *normalized* diffuse and specular direction vectors \vec{d} and \vec{s} .

signal level and standard deviation. Variations from the first two sources are correlated in the different multispectral bands and increase the correlation coefficients of Figure 7. Another source to take into account is the shot noise that results from the quantum nature of light and imposes a linear relationship between signal level and *variance*.

The big peaks in the standard deviation at a highlight are caused by surface roughness, for specular reflection is much more sensitive to variation in local geometry than diffuse reflection. A linear relationship between signal level and standard deviation is imposed by this source. Its variation is correlated in the different multispectral bands, which leads to the large correlation coefficients at highlights (see Figure 7).

4.2 Propagation into the separated reflection components

The propagation of the radiometric noise into the separated reflection components appears from the standard deviation in Figure 9. Of importance is the increasing standard deviation of the diffuse component near highlights. Because the specular reflection raises the signal level in all multispectral bands (see Figure 5), the standard deviations of the signal-dependent noise sources increase. This leads to an increasing standard deviation for both the specular and the diffuse component, because shot noise and spatial variation of the filter transmittance are uncorrelated in the different multispectral bands. Also chromatic aberration of the camera lens can cause such colour shifts at image positions where irradiance changes fast. Averaging over multiple realizations to tackle shot noise and a calibration procedure for lens and filters may reduce the observed effect.

The correlation coefficient from Figure 10 turns out to be small at the highlight, which implies that the *covariance* between the diffuse and specular component stays relatively small for any reflection geometry. Around highlights the reflection component separation strongly *decorrelates* the radiometric noise from the multispectral bands of the image, because the noise source of most significance is surface roughness in those areas, varying the measure-

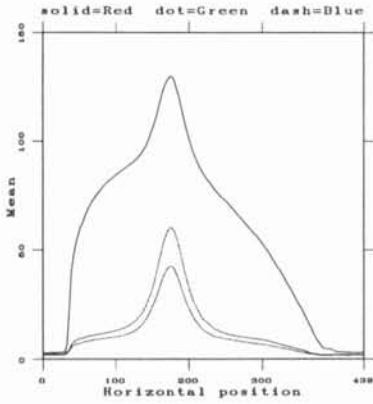


Figure 5: Mean of multispectral image bands.

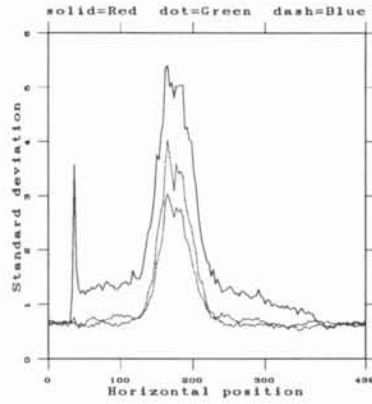


Figure 6: Standard deviation of multispectral image bands.

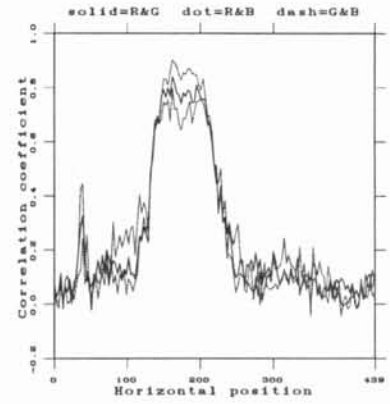


Figure 7: Correlation coefficient between multispectral bands.

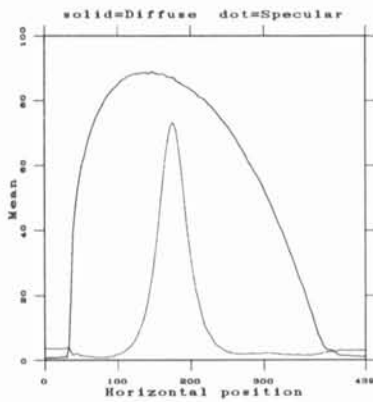


Figure 8: Mean of separated reflection components.

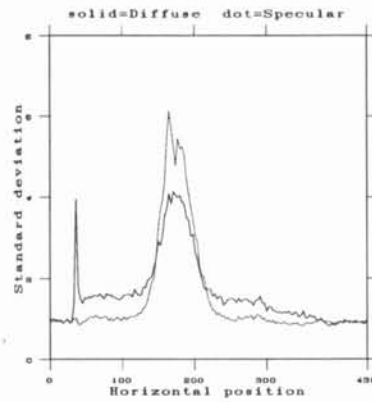


Figure 9: Standard deviation of separated reflection components.



Figure 10: Correlation coefficient between reflection components.

ment vector along the specular direction of feature space.

5 Conclusions

A multispectral camera measurement system has been presented. The images captured from a cylindrical body were successfully separated into reflection components. This set-up provides us with statistical parameters of the radiometric noise as function of the reflection geometry. These statistics can be used to develop a radiometric noise model for the estimation of 3-D body parameters with separated reflection components.

A qualitative analysis learns that the additive noise model is not adequate around highlights. The signal level of each multispectral band of the image is significantly higher in those areas, which enables several signal-dependent noise sources to produce much higher standard deviations. Modeling the variance of the separated reflection components as second order polynomial functions of the multispectral irradiance will be more appropriate. The assumption that the noise is uncorrelated between the separated reflection components seems an acceptable simplifica-

tion, if systematic separation errors can be avoided.

References

- [1] J.C. Glas, F. van der Heijden, "The Use of Separated Reflection Components in Estimating Geometrical Parameters of Curved Surface Elements", *Proc. 5th IEE Conf. Image Proc. Appl.*, Edinburgh, UK, pp. 340-344, July 1995.
- [2] J.C. Glas, F. van der Heijden, "Estimating 3-D Body Parameters from Reflection Component Separating Imagery: A Performance Analysis", *Proc. IEEE Int. Symp. Comp. Vision*, Coral Gables, Florida, USA, pp. 413-418, November 1995.
- [3] S. Tominaga, "Surface Identification Using the Dichromatic Reflection Model", *IEEE Tr. Patt. Anal. Mach. Intell.*, vol. 13, No. 3, pp. 658-670, July 1991.
- [4] G.J. Klinker, "A Physical Approach to Color Image Understanding", Ph.D. Thesis, Carnegie Mellon University, USA, 1988.
- [5] H.W. Sorensen, *Parameter Estimation, Principles and Problems*, Control and Systems Theory, vol. 9, Marcel Dekker, New York, USA, 1980.
- [6] G. Wyszecki, W.S. Stiles, *Color Science: Concepts and Methods, Quantitative Data and Formulae*, Second Edition, John Wiley & Sons, New York, USA, 1982.
- [7] G.E. Healey, R. Kondepudy, "Radiometric CCD Camera Calibration and Noise Estimation", *IEEE Tr. Patt. Anal. Mach. Intell.*, vol. 16, No. 3, pp. 267-276, March 1994.